Biomaterials 84 (2016) 250–261

Contents lists available at ScienceDirect

Biomaterials

journal homepage: www.elsevier.com/locate/biomaterials

Hyaluronic acid-shelled acid-activatable paclitaxel prodrug micelles effectively target and treat CD44-overexpressing human breast tumor xenografts *in vivo*

Yinan Zhong [a], Katharina Goltsche [b], Liang Cheng [a, c], Fang Xie [a, d], Fenghua Meng [a, **], Chao Deng [a], Zhiyuan Zhong [a, *], Rainer Haag [b]

[a] Biomedical Polymers Laboratory, and Jiangsu Key Laboratory of Advanced Functional Polymer Design and Application, College of Chemistry, Chemical Engineering and Materials Science, Soochow University, Suzhou, 215123, PR China
[b] Institut für Chemie und Biochemie, Freie Universität Berlin, Takustraße 3, 14195 Berlin, Germany
[c] Department of Pharmaceutics, College of Pharmaceutical Sciences, Soochow University, Suzhou 215123, PR China
[d] Department of Pathology, School of Biology and Basic Medical Sciences, Soochow University, Suzhou, 215123, PR China

ARTICLE INFO

Article history:
Received 1 December 2015
Received in revised form
21 January 2016
Accepted 21 January 2016
Available online 23 January 2016

Keywords:
pH-sensitive
Hyaluronic acid
Prodrug micelles
Targeted chemotherapy
Human breast cancer

ABSTRACT

The therapeutic efficacy of nanoscale anticancer drug delivery systems is severely truncated by their low tumor-targetability and inefficient drug release at the target site. Here, we report the design and development of novel endosomal pH-activatable paclitaxel prodrug micelles based on hyaluronic acid-*b*-dendritic oligoglycerol (HA-dOG-PTX-PM) for active targeting and effective treatment of CD44-overexpressing human breast cancer xenografts in nude mice. HA-dOG-PTX-PM had a high drug content of 20.6 *wt.*% and an average diameter of 155 nm. The release of PTX was slow at pH 7.4 but greatly accelerated at endosomal pH. MTT assays, flow cytometry and confocal experiments showed that HA-dOG-PTX-PM possessed a high targetability and antitumor activity toward CD44 receptor over-expressing MCF-7 human breast cancer cells. The *in vivo* pharmacokinetics and biodistribution studies showed that HA-dOG-PTX-PM had a prolonged circulation time in the nude mice and a remarkably high accumulation in the MCF-7 tumor (6.19%ID/g at 12 h post injection). Interestingly, HA-dOG-PTX-PM could effectively treat mice bearing MCF-7 human breast tumor xenografts with little side effects, resulting in complete inhibition of tumor growth and a 100% survival rate over an experimental period of 55 days. These results indicate that hyaluronic acid-shelled acid-activatable PTX prodrug micelles have a great potential for targeted chemotherapy of CD44-positive cancers.

1. Introduction

Nanoscale anticancer drug delivery systems have received a widespread interest for targeted caner chemotherapy [1,2]. Their therapeutic efficacy is, however, severely truncated by their low tumor-targetability and/or inefficient drug release at the target site [3–6]. It goes without saying that macromolecular prodrugs and micellar drugs are among the most studied nanomedicines, several of which are currently in the clinical trials [7–10]. The macromolecular prodrugs display usually inferior tumor accumulation and targetability due to a small particle size, while micellar drugs are often associated with low drug loading, low stability and premature drug release. In the past years, a few studies have shown that prodrug micelles could elegantly combine the advantages while overcome the disadvantages of both macromolecular prodrugs and micellar drugs [11–14]. Some of the micellar prodrugs were applied in various tumor models *in vivo*. Hennink et al. reported that doxorubicin (DOX) prodrug micelles based on DOX methacrylamide (DOX-MA) and poly(ethylene glycol)-*b*-poly(N-(2-hydroxypropyl) methacrylamide-lactate) brought about a better tumor growth inhibition and survival rate than free DOX in mice bearing B16F10 melanoma [15]. Kataoka et al. found that (1,2-diaminocyclohexane) platinum (II)-conjugated cRGD-functionalized PEG-*b*-poly(L-glutamic acid) micelles (20% cRGD/m) could bypass vascular/tumor barriers in situ, penetrate deep

* Corresponding author.
** Corresponding author.
E-mail addresses: fhmeng@suda.edu.cn (F. Meng), zyzhong@suda.edu.cn (Z. Zhong).

http://dx.doi.org/10.1016/j.biomaterials.2016.01.049
0142-9612/

into glioblastoma, and produce significant antitumor effects in an orthotopic mouse model of U87MG-Luc2 human glioblastoma [16].

Paclitaxel (PTX) is one of the most important chemotherapeutic agents used in the clinics for the treatment of various cancers including breast, lung and advanced ovarian cancers [17,18]. PTX prodrugs were prepared by conjugating PTX to water soluble polymers such as poly(ethylene glycol) (PEG), poly(N-(2-hydroxypropyl)-methacrylamide) (PHPMA), poly(L-glutamic acid) (PGlu) and hyaluronic acid via a cleavable peptide, ester or phosphonate bond [19–22]. The antitumor activity of PTX prodrugs was generally low partly due to slow intracellular drug release as well as structural modification of PTX (*i.e.* released drug is not pristine PTX). Notably, acetal-linked PTX prodrug micelles based on PEG-*b*-poly(acrylic acid) (PEG-PAA) backbone showed significantly accelerated drug release at endo/lysosomal pH compared to physiological pH and furthermore released PTX had an intact structure [23]. In the past years, various types of acid-labile nanoparticles based on acetal bonds have been constructed for controlled drug delivery [24–27]. It is interesting to note, however, that thus far few prodrug micelles could efficiently accumulate at the tumor site and be actively internalized by target tumor cells. By installation of targeting ligand such as peptide, protein, and aptamer [28,29], the therapeutic efficacy of prodrug micelles could be largely improved [30–34]. It's well known that HA is a natural polysaccharide, which plays a significant role in the tumorigenesis process. HA has a strong affinity to CD44 receptors that are overexpressed on different cancer cells as well as cancer stem cells, which render it particularly interesting for active tumor targeting delivery of drugs and genes [35–40]. However, over substitution of the carboxylic acid groups in HA would compromise its targetability [41,42].

In this paper, novel hyaluronic acid-shelled acid-activatable PTX prodrug micelles were developed from hyaluronic acid-*b*-dendritic oligoglycerol block copolymer (HA-dOG-PTX-PM) for effective targeting and treatment of xenografted human breast cancer *in vitro* and *in vivo* (Scheme 1). Here, no chemical modification of HA shells was made to warrant a high CD44 targetability and efficient uptake of prodrug micelles by CD44 positive cancer cells via a receptor-mediated mechanism. Dendrimers are a unique type of drug carrier [43–45]. dOG with a well-defined structure and multivalency possesses excellent biocompatibility and allows high drug conjugation [46–48]. Importantly, PTX would be quickly released inside the tumor cells as a result of acetal cleavage in the endo/lysosomal compartments. Our results showed that treatment with HA-dOG-PTX-PM led to 100% survival in the nude mice bearing MCF-7 human breast cancer xenografts. To the best of our knowledge, this is a first report on smart paclitaxel prodrug micelles that combine multiple functions including high drug content, active tumor-targeting, and fast intracellular drug release.

2. Materials and methods

2.1. Materials

Methanesulfonyl chloride (MsCl, 99.5%, Acros), sodium azide (NaN_3, 99%, Acros), succinic anhydride (99%, Sigma–Aldrich), 2-chloroethyl vinyl ether (99%, Sigma–Aldrich), *p*-toluenesulfonic acid monohydrate (*p*-TSA, 97.5%, Acros), paclitaxel (PTX, 99%, Beijing Zhongshuo Pharmaceutical Technology Development Co. Ltd.), hyaluronic acid (HA, molecular weight: 9.5 kDa, Shandong Freda Biopharm Co., Ltd.), propargylamine (98%, Sigma–Aldrich), sodium cyanoborohydride ($NaCNBH_3$, 99%, Acros), cupric sulfate ($CuSO_4$, 99%, Sigma–Aldrich), L-ascorbic acid sodium salt (99%, Acros), toluene, N,N-dimethyl formamide (DMF), ethyl acetate, n-hexane, anhydrous methanol, pyridine, dichloromethane (DCM), and anhydrous formamide were used as received. Monoazido dendritic oligoglycerol G1.0-N_3 was synthesized according to a previous report [49].

2.2. Synthesis of dendritic oligoglycerol-paclitaxel (dOG-PTX) conjugate

dOG-PTX conjugate was synthesized from G1.0-N_3 in three steps: (i) treating G1.0-N_3 with succinic anhydride which converts all hydroxyl groups into carboxylic acid groups, (ii) reacting with 2-chloroethyl vinyl ether to obtain N_3-dOG-vinyl ether, and (iii) conjugating with PTX to yield N_3-dOG-PTX in which PTX was linked to dOG via an acetal bond (Scheme 2).

Firstly, G1.0-N_3 (1.0 g, 16.88 mmol hydroxyl group) and succinic anhydride (8.44 g, 84.43 mmol) were reacted in pyridine (10 mL) at 60 °C for 24 h. The resulting conjugate N_3-dOG-COOH was isolated by column chromatography (methanol/dichloromethane). Yield: 84%. Then, under an nitrogen atmosphere, to an anhydrous DMF solution (15 mL) of N_3-dOG-COOH (1 g, 6.28 mmol of carboxyl group) and KOH (1.0 g, 17.86 mmol), a solution of 2-chloroethyl vinyl ether (1.34 g, 12.56 mmol) in anhydrous DMF (5 mL) was added. The reaction was allowed to proceed at room temperature (r.t.) for 24 h. N_3-dOG-vinyl ether conjugate was isolated by distilling off excess 2-chloroethyl vinyl ether and DMF, dissolving in water, extracting with ethyl acetate (3 × 20 mL), and drying *in vacuo*. Yield: 68%. Finally, under a nitrogen flow, to a 25 mL Schlenk flask equipped with a magnetic stirrer were added N_3-dOG-vinyl ether (100 mg, 440 μmol of vinyl ether units), PTX (450 mg, 528 μmol), *p*-TSA (7.6 mg, 44 μmol), 4 Å molecular sieve (1 g) and anhydrous DMF (10 mL). The flask was sealed and the reaction was carried out under stirring at 50 °C for 4 days. The reaction mixture was filtered to remove the molecular sieves. The filtrate was dialyzed against 250 mL of DMF (Spectra/Pore, MWCO 3500) for 24 h with 5 times change of DMF to remove the unreacted PTX. The final product was obtained by dialysis against 500 mL of DI water with 5 times change of water followed by lyophilization for 48 h. Yield: 75%. ^{1}H NMR (CD_3OD): δ 3.61, 3.73, 4.20 and 4.45 (dOG); 2.58 (succinic ester); 3.65 and 4.28 (ethyl ether); 1.36 and 4.37 (acetal bond); 1.11–1.25, 2.03–2.42, 3.52–3.87, and 7.30–8.12 (PTX). M_n (^{1}H NMR) = 2.9 kg/mol. PTX content in the prodrug was determined by ^{1}H NMR and HPLC measurements. PTX content was calculated according to the following formula:

$$\text{PTX content } (wt.\%) = (\text{weight of PTX}/\text{weight of prodrug}) \times 100$$

2.3. Synthesis of HA-dOG-PTX conjugate

HA-dOG-PTX conjugate was obtained by click reaction between HA-alkynyl and N_3-dOG-PTX. HA-alkynyl was prepared by reacting HA (3.0 g, 0.33 mmol) and propargylamine (35.8 mg, 0.65 mmol) in 20 mL of D.I. water in the presence of $NaCNBH_3$ (40.6 mg, 0.65 mmol) at 60 °C for 2 d and then 40 °C for 2 d under a nitrogen atmosphere. HA-alkynyl adduct was isolated by extensive dialysis (Spectra/Pore, MWCO 3500) against D.I. water followed by lyophilization. Yield: 89%. The click reaction was carried out under a nitrogen atmosphere by adding a formamide solution (5.0 mL) of HA-propargylamine (460 mg, 50 μmol), 0.3 mL of aqueous $CuSO_4$ (0.5 mg, 3.4 μmol) solution, and 0.3 mL of aqueous sodium ascorbate (0.8 mg, 4 μmol) solution to a stirred DMF solution (1.0 mL) of N_3-dOG-PTX (100 mg, 34 μmol) followed by reacting at 50 °C for 12 h. The final product was isolated by precipitation in D.I. water, filtration, extensive washing with saturated aqueous EDTA solution and D.I. water to remove unreacted HA-propargylamine, $CuSO_4$,

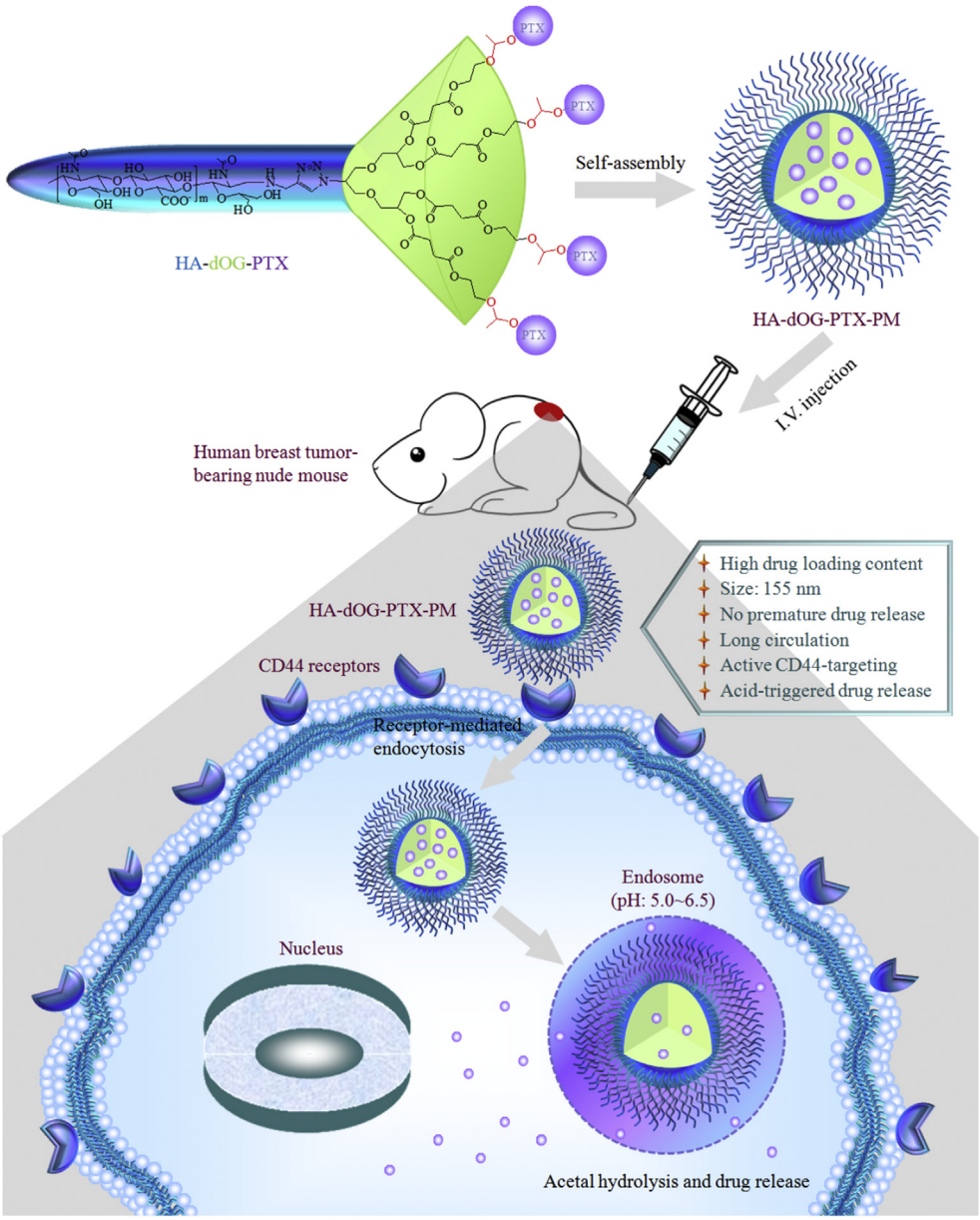

Scheme 1. Endosomal pH-activatable HA-dOG-PTX-PM for active CD44-targeted PTX delivery *in vivo*. (i) HA-dOG-PTX conjugate with a drug content of 20.6 wt.% is self-assembled into core–shell micelles in water; (ii) HA-dOG-PTX-PM has low drug leakage, prolonged circulation time, and high accumulation in the tumor; (iii) HA-dOG-PTX-PM is efficiently taken up by CD44-overexpressing cancer cells via a receptor-mediated endocytosis mechanism; and (iv) inside the tumor cells, PTX is quickly released as a result of acetal cleavage in the endo/lysosomal compartments, resulting in superior anticancer effect *in vivo*.

and sodium ascorbate if present, and drying by lyophilization. Yield: 72%. ^{1}H NMR (D_2O/CD_3OD): 1.86, 2.89, 3.28–4.02, and 4.21–4.75 (HA); 3.61, 3.73, 4.20 and 4.45 (dOG); 2.58 (succinic ester); 3.65 and 4.28 (ethyl ether); 1.36 and 4.37 (acetal bond); 1.11–1.25, 2.03–2.42, 3.52–3.87, and 7.30–8.12 (PTX). ^{1}H NMR showed equivalent coupling of HA and N_3-dOG-PTX by comparing the integrals of signals at δ 1.86 (*N*-acetyl protons in HA) and 7.30–8.12 (aromatic protons in PTX). M_n (^{1}H NMR) = 12.1 kg/mol.

2.4. Characterization

^{1}H NMR spectra were recorded on a Bruker ECX 400 spectrometer operating at 400 MHz using CD_3OD, D_2O or D_2O/CD_3OD (1/1, v/v) mixture as a solvent. The chemical shifts were calibrated against residual H_2O solvent signal. The size of micelles was determined using dynamic light scattering (DLS) at 25 °C using Zetasizer Nano-ZS (Malvern Instruments) equipped with a 633 nm He–Ne laser using back-scattering detection. Transmission electron microscopy (TEM) was performed using a Tecnai G220 TEM operated at an accelerating voltage of 200 kV. The samples were prepared by dropping 10 μL of 0.2 mg/mL micelle suspension on the copper grid followed by staining with phosphotungstic acid (1 *wt.* %). The amount of PTX was determined by HPLC (Waters 1525) with UV detection at 227 nm using acetonitrile/water (1/1, v/v) as a mobile phase.

2.5. Preparation of PTX prodrug micelles

Prodrug micelles were prepared by dropwise addition of 4.0 mL of phosphate buffer (PB, pH 7.4, 10 mM) to a formamide solution

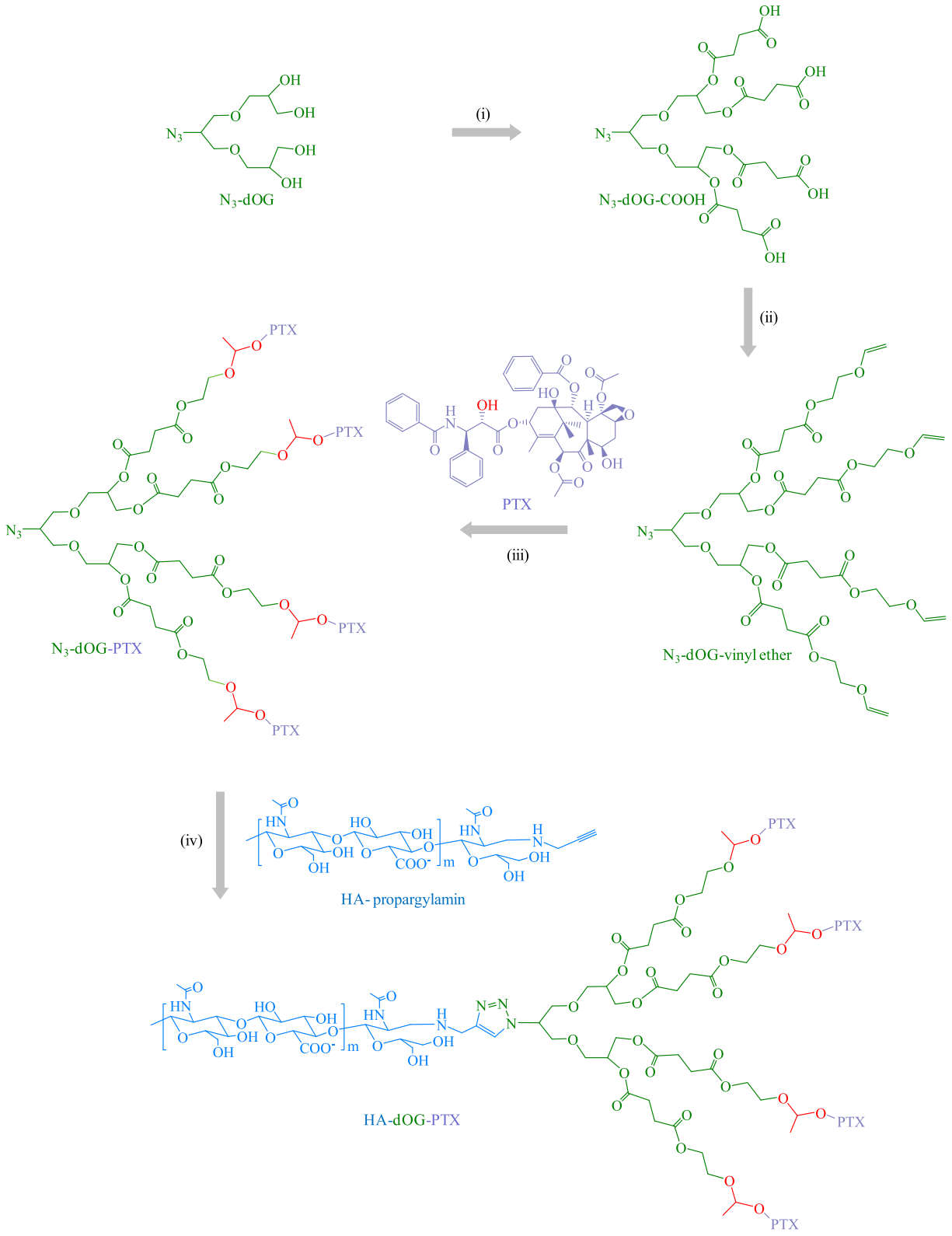

Scheme 2. Synthetic pathway for HA-dOG-PTX conjugate. Conditions: (i) succinic anhydride, pyridine, 60 °C, 24 h; (ii) 2-chloroethyl vinyl ether, KOH, DMF, r.t., 24 h; (iii) PTX, p-TSA, 4 Å molecular sieve, DMF, 50 °C, 96 h; (vii) HA-propargylamin, $CuSO_4$, sodium ascorbate, DMF/H_2O, 50 °C, 12 h.

(1.0 mL) of HA-dOG-PTX (5 mg/mL) under stirring at r.t., followed by extensive dialysis (Spectra/Pore, MWCO 3500) against PB (pH 7.4, 10 mM) for 24 h. The critical micelle concentration (CMC) was determined using pyrene as a fluorescence probe. The concentration of the conjugates was varied from 1.0×10^{-5} to 0.1 mg/mL and the concentration of pyrene was fixed at 1.0 μM. The fluorescence spectra were recorded using a FLS920 fluorescence spectrometer with the excitation wavelength of 330 nm. The

emission fluorescence at 372 and 383 nm were monitored. The CMC was estimated as the cross-point when extrapolating the intensity ratio I_{372}/I_{383} at low and high concentration regions.

2.6. In vitro drug release from PTX prodrug micelles

The drug release from PTX prodrug micelles (HA-dOG-PTX-PM) was studied using a dialysis tube (Spectra/Pore, MWCO 12000) at 37 °C in three different media, *i.e.* pH 5.0 (acetate buffer, 10 mM), pH 6.0 (acetate buffer, 10 mM), and pH 7.4 (PB, 10 mM). Drug release studies were performed with 0.6 mL of HA-dOG-PTX-PM dispersion dialysis against 20 mL of the corresponding medium. At desired time intervals, 6.0 mL of release medium was taken out and replenished with an equal volume of fresh medium. The amount of PTX released was determined by HPLC measurement. The release experiments were conducted in triplicate, and the results presented were the average data with standard deviations.

2.7. In vitro cytotoxicity assays

The cytotoxicity of HA-dOG prepolymer was determined using MCF-7 human breast cancer cells that express a high level of CD44 receptors. The cells were plated in a 96-well plate (1×10^4 cells/well) using RPMI 1640 media supplemented with 10% fetal bovine serum, 1% L-glutamine, antibiotics penicillin (100 IU/mL) and streptomycin (100 μg/mL). After 24 h, prescribed amounts of HA-dOG in 20 μL of PBS were added (final micelle concentrations were fixed at 0.5 and 1.0 mg/mL) and incubated in an atmosphere containing 5% CO_2 for 48 h at 37 °C. In addition, acetaldehyde, which is a hydrolysis byproduct of PTX prodrug micelles, was also added at a concentration of 14.9 μM (corresponding to a maximal amount of acetaldehyde generated from 1.0 mg/mL of HA-dOG-PTX-PM). Then, 3-(4,5-dimethylthiazol-2-yl)-2,5-diphenyl tetrazoliumbromide (MTT) solution in PBS (20 μL, 5 mg/mL) was added. After incubation for 4 h, the supernatant was carefully aspirated, and the MTT-formazan generated by live cells was dissolved in 150 μL of DMSO for 20 min. The absorbance at a wavelength of 490 nm was measured using a microplate reader (Bio-Tek, ELX808IU). The cell viability (%) was determined by comparing the absorbance at 490 nm with control wells containing only cell culture medium. The experiments were performed in quartets.

The antitumor activities of HA-dOG-PTX-PM and Taxol (PTX in Cremophor EL and ethanol, v/v = 1:1) were also studied by MTT assays. Briefly, the cells were plated in a 96-well plate (1×10^4 cells/well) using RPMI 1640 media supplemented with 10% fetal bovine serum, 1% L-glutamine, antibiotics penicillin (100 IU/mL) and streptomycin (100 μg/mL). After 24 h, prescribed amounts of HA-dOG-PTX-PM or Taxol at PTX concentrations ranging from 7.5×10^{-4} to 25.0 μg/mL in 20 μL of PBS were added and incubated in an atmosphere containing 5% CO_2 for 4 h at 37 °C, the medium was aspirated and replaced by fresh medium, and the cells were incubated in an atmosphere containing 5% CO_2 for another 48 h at 37 °C. MTT solution in PBS (20 μL, 5 mg/mL) was added. After incubation for 4 h, the supernatant was carefully aspirated, and the MTT-formazan generated by live cells was dissolved in 150 μL of DMSO for 20 min. The cell viabilities were determined by MTT assays as described above. The inhibition experiments were performed by pre-treating MCF-7 cells with free HA (5 mg/mL) for 4 h prior to incubating with HA-dOG-PTX-PM.

2.8. Flow cytometry and confocal microscopy measurements

The cellular uptake and intracellular drug release behaviors of HA-dOG-PTX-PM were studied in MCF-7 cells by loading DOX into the micelles to trace DOX fluorescence using flow cytometry and confocal laser scanning microscopy (CLSM). DOX could be physically loaded into HA-dOG-PTX-PM by dropwise addition of 4 mL of PB (10 mM, pH 7.4) to a mixture of HA-dOG-PTX polymer (1.0 mL, 5 mg/mL) in formamide and DOX (250 μL, 5 mg/mL) in DMSO under stirring at r.t., followed by dialysis against PB (10 mM, pH 7.4) for 24 h (Spectra/Pore, MWCO 3500). The cells were seeded in a 6-well plate (1×10^6 cells/well) using RPMI 1640 media containing 10% fetal bovine serum, 1% L-glutamine, antibiotics penicillin (100 IU/mL), and streptomycin (100 μg/mL) for 12 h. DOX-loaded HA-dOG-PTX-PM or DOX·HCl in 400 μL of phosphate buffered saline (PBS) was added to each well (10.0 μg DOX/mL). After incubation at 37 °C for 2 or 4 h, the cells were digested by 0.25% (w/v) trypsin and 0.03% (w/v) EDTA. The suspensions were centrifuged at 700 × g for 5 min at 4 °C, washed twice with PBS, and then re-suspended in 500 μL of PBS. Fluorescence histograms were then recorded with a BD FACSCalibur flow cytometer (Beckton Dickinson, USA) and analyzed using Cell Quest software. We analyzed 20,000 gated events to generate each histogram. The gate was arbitrarily set for the detection of red fluorescence. The inhibition experiments were performed by pre-treating MCF-7 cells with free HA (5 mg/mL) for 4 h prior to incubating with DOX-loaded HA-dOG-PTX-PM.

For confocal studies, MCF-7 cells were cultured on microscope slides in a 24-well plate (5×10^4 cells/well) using RPMI 1640 media containing 10% fetal bovine serum, 1% L-glutamine, antibiotics penicillin (100 IU/mL) and streptomycin (100 μg/mL). After 24 h, DOX-loaded HA-dOG-PTX-PM or DOX·HCl in 100 μL of PBS was added to each well (DOX dosage: 10.0 μg/mL). After 2 or 10 h incubation, the culture medium was removed and the cells on microscope plates were washed three times with PBS. The cells were fixed with 4% paraformaldehyde solution for 20 min and washed with PBS containing 0.1% triton X-100 for three times. The cytoskeleton was stained with fluorescein isothiocyanate-labeled phalloidine (phalloidine-FITC, green) for 1 h and washed with PBS for three times. The cell nuclei were stained with 4′,6-diamidino-2-phenylindole (DAPI, blue) for 20 min and washed with PBS for three times. The fluorescence images were obtained using confocal microscope (TCS SP2). The inhibition experiments were performed by pre-treating MCF-7 cells with free HA (5 mg/mL) for 4 h prior to incubating with DOX-loaded HA-dOG-PTX-PM.

2.9. Blood circulation and in vivo imaging

The mice were handled under protocols approved by Soochow University Laboratory Animal Center and the Animal Care and Use Committee of Soochow University. The PTX level in blood was measured by withdrawing ~10 μL of blood from the tail vein of nude mice at different time points post-injection of HA-dOG-PTX-PM and Taxol (10 mg PTX equiv./kg). Each blood sample was dissolved in 0.3 mL of methanol containing acetic acid with brief sonification. PTX was extracted by incubating blood samples overnight followed by centrifugation at 10,000 rpm for 10 min. The supernatant was taken and evaporated to dryness under a stream of nitrogen. 100 μL of acetonitrile was added to re-dissolve the residue and the amount of PTX was determined by HPLC. The blood circulation followed a typical two compartment model. The first phase is distribution phase with usually a rapid decline. The second phase is elimination phase with usually a long period, which is the predominant process for drug clearance. We calculated the half-lives of two phases (t_1, and t_2) according to the following formula:

$$y = A_1 \times \exp(-x/t_1) + A_2 \times \exp(-x/t_2) + y_0$$

In order to monitor drug release from micelles using fluorescence imaging *in vivo*, fluorescent molecule DIR was loaded into HA-dOG-PTX-PM. Human breast tumor xenograft model was

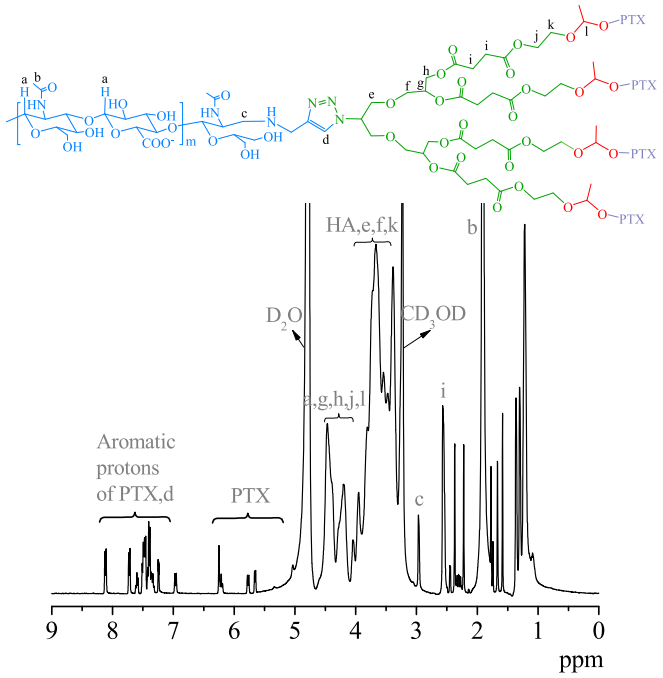

Fig. 1. ^{1}H NMR spectrum (400 MHz, CD_3OD/D_2O) of HA-dOG-PTX.

established by subcutaneous inoculation of 1×10^7 MCF-7 cells in 50 μL serum-free RPMI 1640 media into the hind flank of each mouse. When the size of tumors reached about 200 mm^3, DIR-loaded HA-dOG-PTX-PM was injected via tail vein. The fluorescent scans were performed at various time points (1, 4, 8, 12, 24 and 48 h) post *i.v.* injection using the Maestro *in vivo* fluorescence imaging system (CRi Inc.).

2.10. In vivo biodistribution studies

Taking advantage of the fluorescent nature of DIR, *ex vivo* fluorescence imaging was performed using DIR-loaded HA-dOG-PTX-PM. A single dose of DIR-loaded HA-dOG-PTX-PM in 0.2 mL of PBS was administrated intravenously via the tail vein. After 12 h, MCF-7 tumor-bearing mice were sacrificed. The tumor block and several major organs including heart, liver, spleen, lung, and kidney were collected, washed, and dried. Fluorescence images were acquired with the Maestro *in vivo* fluorescence imaging system (CRi Inc.).

To quantify the amount of PTX delivered to the tumor and different organs, tumor-bearing mice following 12 h injection with HA-dOG-PTX-PM or Taxol (10 mg PTX equiv./kg) were sacrificed. The tumor block and organs including heart, liver, spleen, lung, and kidney were collected, washed, weighed, and then homogenized in 0.5 mL of methanol containing acetic acid to extract PTX using homogenizer (IKA T25) followed by incubation overnight and then centrifugation at 10,000 rpm for 10 min. The supernatant was taken and evaporated to dryness under a stream of nitrogen. 100 μL of acetonitrile was added to re-dissolve the residue and the amount of PTX was determined by HPLC.

2.11. In vivo antitumor efficacy

MCF-7 tumor-bearing mice were treated with HA-dOG-PTX-PM and Taxol at a dosage of 5.0 mg PTX equiv./kg. The drugs were intravenously injected every three days. PBS was used as a blank control. The tumor sizes were measured by calipers every three days and volume was calculated according to the formula $V = 0.5 \times L \times W \times H$, wherein L is the tumor dimension at the longest point, W is the tumor dimension at the widest point, and H is the tumor dimension at the highest point. Relative tumor volumes were calculated as V/V_0 (V_0 is the tumor volume when the treatment was initiated). Mice were weighed with the relative body weights normalized to their initial weights. Mice in each cohort were considered to be dead either when the tumor volume increased to 1000 mm^3 or when the mice died during treatment.

2.12. Maximum tolerated dose

Female nude mice (at 6–7 weeks of age) were used to evaluate the maximum tolerated dose (MTD) of Taxol and HA-dOG-PTX-PM. Three groups of mice received a single dose of HA-dOG-PTX-PM by intravenous injection at a dosage of 20, 50, and 100 mg/kg PTX, respectively. Another three groups of mice received Taxol at a dosage of 10, 15, and 20 mg/kg PTX, respectively. The control groups received saline only. The body weight and physical states of all the mice were monitored for a period of 14 d. The MTD was defined as the allowance of a median body weight loss of 15% and causes neither death due to toxic effects nor remarkable changes in the general signs within 14 d after administration [50].

2.13. Histological analysis

At the end of the treatment (day 30), one mouse of each group was sacrificed. The tumor and liver were excised, fixed with paraformaldehyde for 48 h, embedded in paraffin, and cut into 5 μm thin slices. The tissue slices were stained by hematoxylin and eosin (H&E) and observed by a digital microscope (Leica QWin). For TUNEL experiments, tumor slices were treated with FragELTM DNA fragment detection kit (colorimetric-TdT Enzyme method) according to the manufacturer's protocol (EMD chemicals Inc, Darmstadt, Germany) followed by observation under light microscopy.

3. Results and discussion

3.1. Synthesis of HA-dOG-PTX conjugate

HA-dOG-PTX conjugate was prepared via click reaction between HA-alkynyl and N_3-dOG-PTX (Scheme 2). N_3-dOG-PTX was obtained in following three steps: (i) treatment of N_3-dOG-OH with succinic anhydride, converting periphery hydroxyl group into carboxylic acid group; (ii) reaction of N_3-dOG-COOH with 2-chloroethyl vinyl ether yielding N_3-dOG-vinyl ether; and (iii) conjugation of PTX to N_3-dOG-vinyl ether obtaining N_3-dOG-PTX. The introduction of succinic ester and vinyl ether would largely decrease the steric hindrance when conjugating with PTX. ^{1}H NMR of N_3-dOG-COOH showed besides signals owing to N_3-dOG-OH (δ 3.61, 3.73, 4.20 and 4.45) a new signal at δ 2.58 attributable to succinic ester moiety (Fig. S1). The intensity ratio of signals at δ 2.58 (succinic proton) and 4.45 was close to 4/1, indicating quantitative succinic modification of N_3-dOG-OH. ^{1}H NMR of N_3-dOG-vinyl ether displayed new peaks at δ 3.93, and 6.47, which were the characteristic signals of vinyl group (Fig. S2). In addition, the integrals at δ 6.47 (vinyl proton) and 2.58 (succinic proton) displayed a ratio of 1/4, confirming 100% conversion of hydroxyl group into vinyl ether (Fig. S2). PTX was readily conjugated to N_3-dOG-vinyl ether via an acetal bond through a click-type reaction between 2′-hydroxyl group of PTX and the periphery vinyl ether as our previous report [23]. ^{1}H NMR showed besides peaks of N_3-dOG-vinyl ether also signals due to PTX at δ 1.11–1.25, 2.03–2.42, 3.52–3.87, and 7.30–8.12 (Fig. S3). The percentage of PTX conjugated to N_3-dOG-vinyl ether was calculated, by comparing integrals of signals at

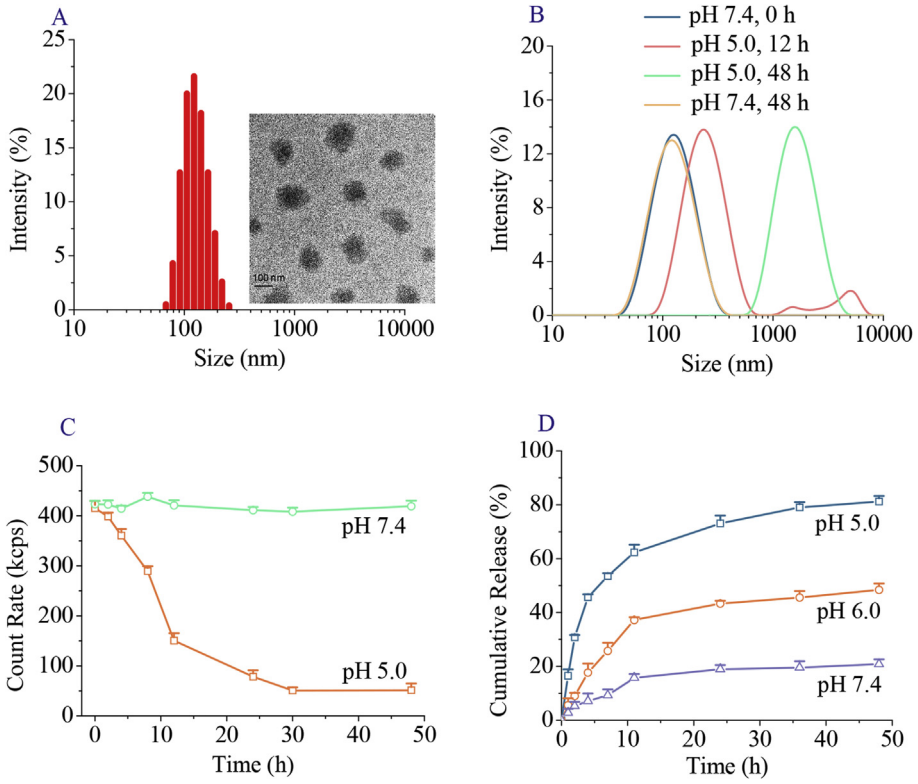

Fig. 2. Characteristics of HA-dOG-PTX-PM. (A) Size distribution measured by DLS, insert is the corresponding TEM micrograph; (B) change of size distribution at pH 5.0 or 7.4 at 37 °C; (C) change of scattering intensity over time at pH 5.0 or 7.4 at 37 °C. The kcps is the mean count rate in kilo counts per second; and (D) pH-dependent drug release from HA-dOG-PTX-PM at 37 °C. Data are presented as mean ± SD (n = 3).

δ 7.30–8.12 (aromatic protons in PTX) with 2.58 (succinic proton), to be 73.0 *wt.* % (Fig. S3). HPLC measurement of N_3-dOG-PTX after complete acid hydrolysis showed a PTX content of 74.2 *wt.* %, close to that determined by ^{1}H NMR.

HA-alkynyl was prepared by reductive amination of HA terminal aldehyde (9.5 kDa) with propargylamine in the presence of $NaCNBH_3$. ^{1}H NMR detected new signals at δ 2.64, and 2.89 attributable to the methylene protons linked to propargylamine moiety (Fig. S4). The comparison of the integrals of signals at δ 2.64 and 2.89 (methylene protons next to propargylamine moiety) with 4.21–4.75 (anomeric proton in HA) showed a ratio of 1/25, indicating quantitative functionalization of HA with alkynyl group (Fig. S4). To further confirm the successful synthesis of HA-alkynyl, a model reaction with acetal-protected G1.0-N_3 was performed. ^{1}H NMR of the isolated adduct showed a new peak characteristic of triazole proton at δ 7.89 and the ratio of the signal intensity at δ 7.89 to that at δ 2.64 and 2.89 (methylene protons next to amine) was about 1/2 (Fig. S5), supporting that HA-alkynyl has a high degree of functionality.

The click reaction between HA-alkynyl and N_3-dOG-PTX was carried out in the presence of $CuSO_4$ and sodium ascorbate at 50 °C in mixed solvent containing formamide, DMF, and D.I. water. The resulting HA-dOG-PTX conjugate was purified by precipitation in D.I. water, filtration, extensive washing with saturated aqueous EDTA solution and D.I. water in sequence. ^{1}H NMR showed besides peaks of N_3-dOG-PTX also signals due to HA at δ 1.86, 2.89, 3.28–4.02, and 4.21–4.75 (Fig. 1). Importantly, the signals at δ 1.86 (methyl protons next to amido linkage of HA) and 7.30–8.12 (aromatic protons of PTX) had an integral ratio of 75/47 (Fig. 1), indicating an equivalent coupling of HA-alkynyl and N_3-dOG-PTX.

3.2. Preparation of HA-dOG-PTX micelles and pH-triggered drug release

Prodrug micelles (PM) were conveniently prepared by solvent exchange method. The dynamic light scattering (DLS) measurements showed that HA-dOG-PTX conjugate formed monodisperse micelles (HA-dOG-PTX-PM) with a mean diameter of 155 nm and a low polydispersity (PDI) of 0.12 (Fig. 2A). As expected, the zeta potential measurement displayed that HA-dOG-PTX-PM possessed a negative surface charge of −21 mV. TEM micrograph demonstrated that HA-dOG-PTX-PM had an average size of ca. 120 nm (Fig. 2A), somewhat smaller than that determined by DLS, likely due to shrinkage of the micelles upon drying. The critical micelle concentration (CMC) determined using pyrene as a fluorescence probe revealed that HA-dOG-PTX-PM had a low CMC of ca. 6.8 mg/L. The micelle size monitored by DLS showed that HA-dOG-PTX-PM swelled from 155 nm to 1800 nm in 48 h at pH 5.0 while little size change was observed at pH 7.4 under otherwise the same conditions (Fig. 2B). The increasing micelle size at pH 5.0 can be attributed to the acidic hydrolysis of acetals, which turns hydrophobic core into more and more hydrophilic. In accordance, the scattering intensities decreased quickly over time at pH 5.0 while remained constant at pH 7.4 (Fig. 2C). The *in vitro* release studies at 37 °C showed that drug release from HA-dOG-PTX-PM was highly dependent on pH, in which ca. 20%, 48% and 81% of PTX was released in 48 h at pH 7.4, pH 6.0 and pH 5.0, respectively (Fig. 2D). Similar results were also reported for acetal-linked PTX prodrug micelles based on PEG-PAA backbone [23]. The acidic hydrolysis of the acetal bonds leads to release of PTX in its native form. These results corroborate that HA-dOG-PTX-PM is highly pH-sensitive and can be readily activated at endo/lysosomal pH.

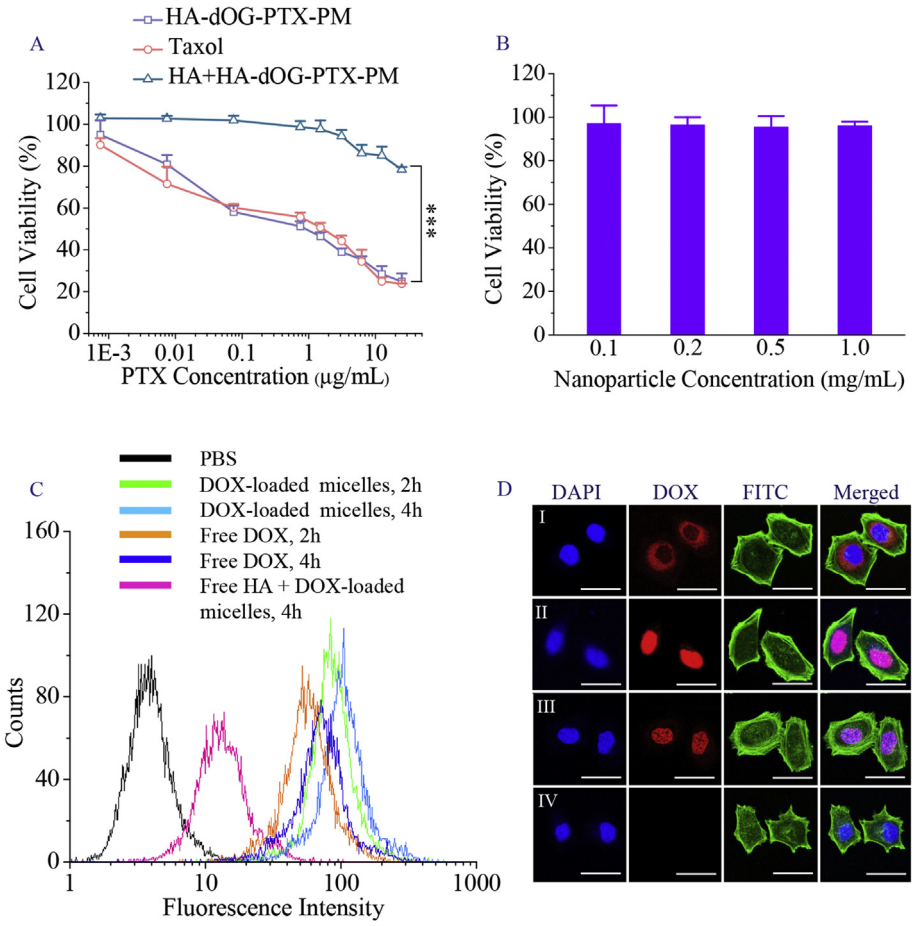

Fig. 3. In vitro characterization of HA-dOG-PTX-PM in MCF-7 cells. (A) The *in vitro* antitumor activity of HA-dOG-PTX-PM. The cells were treated with HA-dOG-PTX-PM for 4 h, the medium was removed and replenished with fresh culture medium, and the cells were incubated for another 48 h. Taxol was used as a control. The inhibition experiment was performed by pre-treating cells for 4 h with free HA polymer (5 mg/mL) prior to incubation with HA-dOG-PTX-PM. Data are presented as mean ± SD (n = 6). $^{*}p < 0.05$, $^{**}p < 0.01$, and $^{***}p < 0.001$ (Student's t test); (B) cytotoxicity of HA-dOG-vinyl ether polymer in the presence of 14.9 μM acetaldehyde in MCF-7 cells following 48 h incubation. Data are presented as the average ± SD (n = 4); (C) flow cytometry of MCF-7 cells following 2 and 4 h incubation with DOX-loaded HA-dOG-PTX-PM (DOX dosage: 10.0 μg/mL). Free DOX was used as a control. The competitive inhibition experiment was performed by pre-treating MCF-7 cells with free HA (5.0 mg/mL) for 4 h before adding DOX-loaded HA-dOG-PTX-PM; and (D) CLSM images of MCF-7 cells following 2 h (I) and 10 h (II) incubation with DOX-loaded HA-dOG-PTX-PM (DOX dosage: 10.0 μg/mL). The cells treated with free DOX for 10 h (III) and cells pre-treated with free HA before adding HA-dOG-PTX-PM for 10 h incubation (IV) were used as controls. For each panel, the images from left to right show cell nuclei stained by DAPI (blue), DOX fluorescence in cells (red), cytoskeleton stained by phalloidine-FITC (green) and overlays of the three images. The scale bar corresponds to 20 μm in all the images. (For interpretation of the references to colour in this figure legend, the reader is referred to the web version of this article.)

3.3. CD44-targeting drug delivery and antitumor activity

The *in vitro* antitumor activity of HA-dOG-PTX-PM was evaluated in CD44 receptor-overexpressing MCF-7 cells by MTT assays. The results showed that HA-dOG-PTX-PM was highly potent against MCF-7 cells with a low half-maximal inhibitory concentrations (IC_{50}) of ca. 0.93 μg PTX equiv./mL, which was lower than that of Taxol (1.63 μg PTX equiv./mL) (Fig. 3A). The competitive experiments revealed that the antitumor activity of HA-dOG-PTX-PM was significantly reduced by pretreating MCF-7 cells with free HA (Fig. 3A), supporting that HA-dOG-PTX-PM is internalized by MCF-7 cells via a receptor-mediated mechanism. The cytotoxicity of HA-dOG-vinyl ether prepolymer was also tested in MCF-7 cells. The cleavage of the acetal bond would yield acetaldehyde. Here, 14.9 μM acetaldehyde, which corresponds to a maximal possible concentration of acetal degradation product from 1.0 mg/mL HA-dOG-PTX-PM, was added to the culture media. The results revealed that HA-dOG-vinyl ether together with 14.9 μM acetaldehyde was basically nontoxic toward MCF-7 cells at varying concentrations from 0.1 to 1.0 mg/mL (Fig. 3B).

In order to study their cellular uptake and intracellular drug release behaviors, HA-dOG-PTX-PM was loaded with fluorescent doxorubicin (DOX) and studied using flow cytometry and confocal laser scanning microscopy (CLSM). As fluorescence of DOX is self-quenched when encapsulated into micelles, DOX fluorescence observed inside cells correlates with the intracellular DOX release [51,52]. Flow cytometry showed that MCF-7 cells following 2 or 4 h incubation with DOX-loaded HA-dOG-PTX-PM had higher intracellular DOX level than those incubated with free DOX under otherwise the same conditions (Fig. 3C), confirming fast uptake of HA-dOG-PTX-PM. The inhibition experiments showed that DOX fluorescence in MCF-7 cells was markedly reduced by pre-treating the cells with free HA prior to incubation with DOX-loaded HA-dOG-PTX-PM (Fig. 3C), further corroborating that HA-dOG-PTX-PM is taken up by MCF-7 cells via a receptor-mediated mechanism. CLSM results showed that DOX fluorescence was detected in the perinuclear region of MCF-7 cells following 2 h incubation with DOX-loaded HA-dOG-PTX-PM and DOX was released into the cell nuclei in 10 h (Fig. 3D). In line with the flow cytometry results, MCF-7 cells treated with DOX-loaded HA-dOG-PTX-PM had an obviously stronger DOX fluorescence than those with free DOX, and negligible DOX fluorescence was detected in the cells pretreated

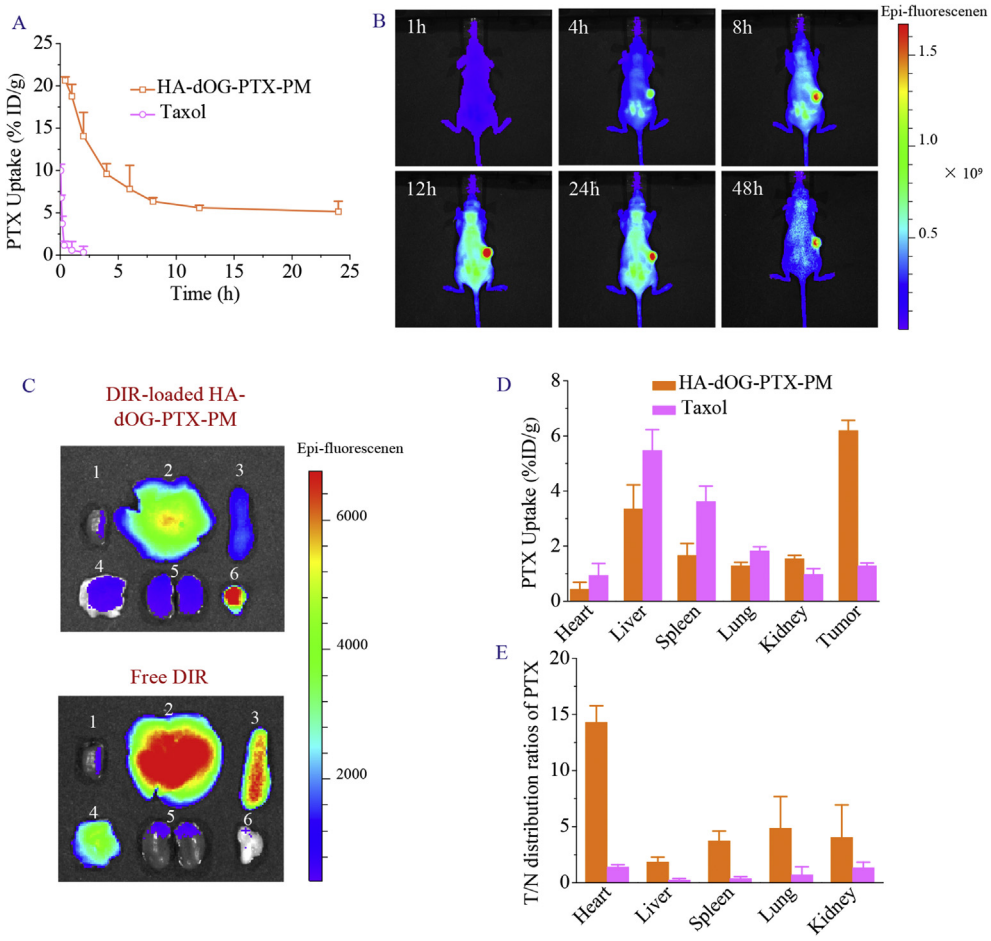

Fig. 4. In vivo pharmacokinetics, imaging, and biodistribution studies. (A) In vivo pharmacokinetics of HA-dOG-PTX-PM and Taxol in mice. PTX levels were determined by HPLC measurements. PTX uptake is expressed as injected dose per gram of tissue (%ID/g). Data are presented as mean ± SD (n = 3); (B) *in vivo* fluorescence images of MCF-7 human breast tumor-bearing nude mice at different time points following injection of DIR-loaded HA-dOG-PTX-PM. The mouse autofluorescence was removed by spectral unmixing using the Maestro software; (C) DIR fluorescence images of tumor and organs (1: heart, 2: liver, 3: spleen, 4: lung, 5: kidney, and 6: tumor); (D) quantification of PTX accumulated in tumor and different organs using HPLC measurements. PTX uptake is expressed as injected dose per gram of tissue (%ID/g). Data are presented as mean ± SD (n = 3); and (E) tumor-to-normal tissue (T/N) distribution ratios of PTX in different organs at 12 h after i.v. injection. Data are presented as mean ± SD (n = 3).

with free HA (Fig. 3D). These results have demonstrated that HA-dOG-PTX-PM can actively target to MCF-7 cells and drug can be quickly released inside the cancer cells. Moreover, HA-dOG-PTX-PM has also shown a great potential for targeted co-delivery of chemotherapeutic agents into CD44 positive cancer cells.

3.4. *In vivo* pharmacokinetics and biodistribution

In the following, we investigated the *in vivo* pharmacokinetics of HA-dOG-PTX-PM in the nude mice. The plasma levels of PTX at different time intervals following a single *i.v.* injection of HA-dOG-PTX-PM or Taxol (10 mg PTX equiv./kg) were determined by HPLC measurements. The results showed that HA-dOG-PTX-PM had a significantly longer circulation time than Taxol, in which the distribution phase half-lives were determined to be 1.63 and 0.12 h, while the elimination phase half-lives were 4.32 and 0.23 h, for HA-dOG-PTX-PM and Taxol, respectively (Fig. 4A). The total area under the curve (AUC) of HA-dOG-PTX-PM was calculated to be 158.4 mg·h/L, which was ca. 68-fold higher than that of Taxol (2.3 mg·h/L), confirming that HA-dOG-PTX-PM has a high stability *in vivo*. Notably, the clinical studies of PTX-incorporating micellar nanoparticles (NK105) showed a 30-fold higher plasma AUC than the commonly used PTX formulation [53].

To evaluate its *in vivo* tumor-targetability, DIR-loaded HA-dOG-PTX-PM was injected intravenously to mice bearing human MCF-7 tumor xenografts and monitored using a Maestro EX *in vivo* fluorescence imaging system (CRi, Inc.). The fluorescence images showed significant tumor accumulation of DIR at 4 h post injection (Fig. 4B). DIR fluorescence intensity in the tumor reached the maximum at 12 h and remained strong even at 48 h post injection, confirming high tumor accumulation and retention of HA-dOG-PTX-PM. Similar results have also been observed for reduction-sensitive reversibly crosslinked hyaluronic acid nanoparticles [41].

The *ex vivo* fluorescence images of tumor and the major organs following 12 h *i.v.* injection of DIR-loaded HA-dOG-PTX-PM revealed much stronger DIR fluorescence in the tumor than in the healthy organs such as liver, spleen, kidney, lung, and heart (Fig. 4C). In comparison, negligible DIR fluorescence in the tumor while strong DIR fluorescence in the liver, spleen, and lung were observed for free DIR-treated mice (Fig. 4C). These results demonstrate that HA-dOG-PTX-PM can significantly improve the biodistribution of DIR *in vivo*. The quantification of PTX using HPLC measurements showed that the tumor uptake of PTX was 6.19% of injected dose per gram of tissue (%ID/g) for HA-dOG-PTX-PM (Fig. 4D), which is notably high as less than 5%ID/g of drug is typically observed in the tumor for both macromolecular prodrugs

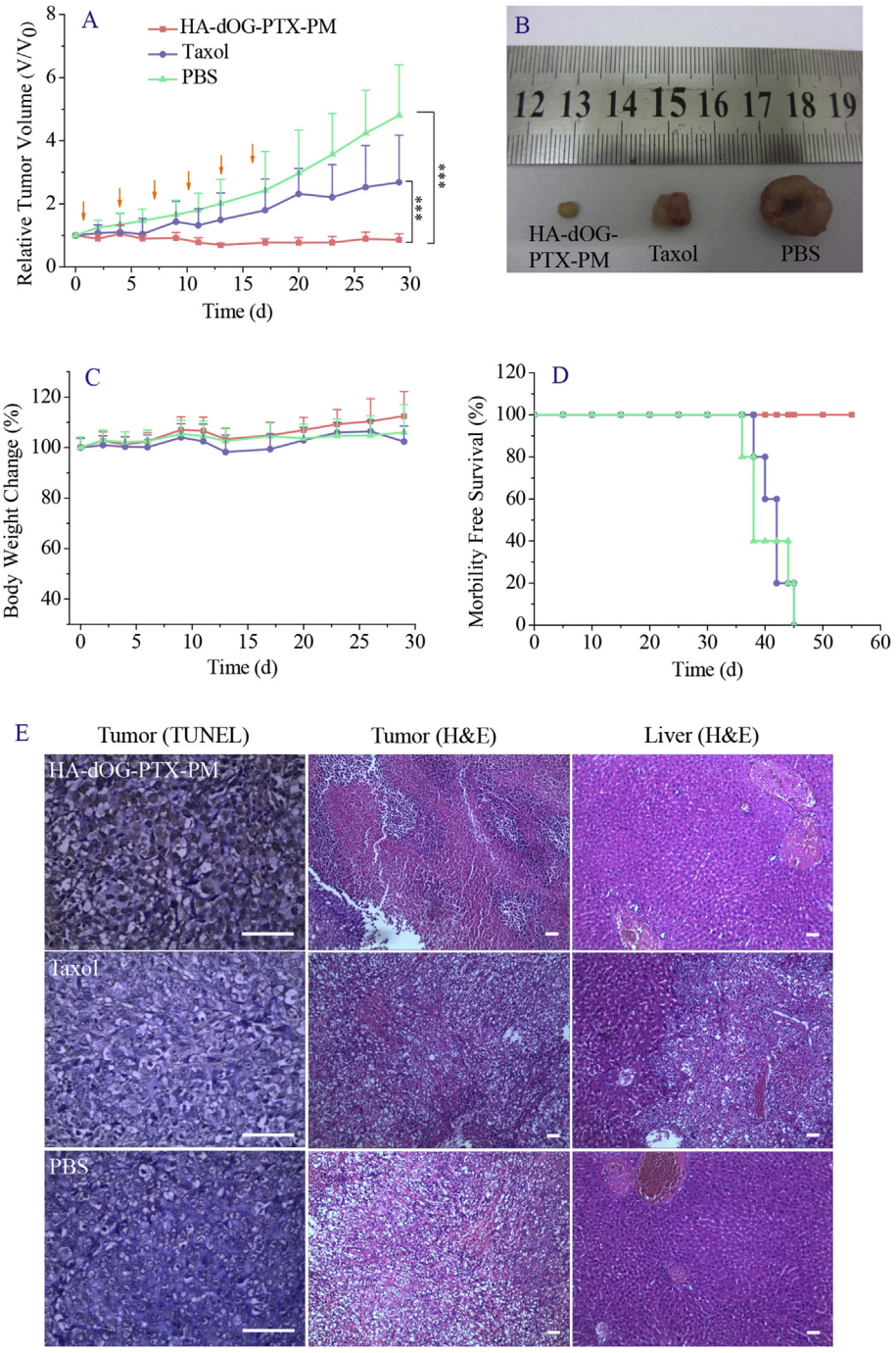

Fig. 5. In vivo antitumor performance of HA-dOG-PTX-PM in MCF-7 human breast tumor-bearing nude mice. (A) Tumor volume changes of mice treated with HA-dOG-PTX-PM, Taxol, and PBS, respectively. The drug was given on day 1, 4, 7, 10, 13, and 16 (dosage: 5.0 mg PTX equiv./kg body weight, in 0.2 mL PBS). Data are presented as mean ± SD (n = 6). $^{*}p < 0.05$, $^{**}p < 0.01$, and $^{***}p < 0.001$ (Student's t test); (B) photographs of typical tumor blocks collected from different treatment groups of mice on day 29; (C) body weight changes of mice in different treatment groups within 29 d. Data are presented as mean ± SD (n = 6); (D) survival rates of mice in different treatment groups within 55 d; and (E) TUNEL, and H&E-staining of tumor section, as well as H&E staining of liver section excised from MCF-7 human breast tumor-bearing mice following 30 d treatment with HA-dOG-PTX-PM. Mice treated with Taxol and PBS were used as controls. The scale bar represents 50 μm.

and micellar drugs [54]. In addition, HA-dOG-PTX-PM displayed decreased accumulation in heart, liver, spleen, and lung as compared with Taxol (Fig. 4D). Fig. 4E presents the tumor-to-normal tissue (T/N) distribution ratios of PTX. Notably, HA-dOG-PTX-PM exhibited significantly higher T/N ratios than Taxol. The uptake of HA-dOG-PTX-PM in the liver was higher than in the other healthy organs. HA nanoparticles were known to result in elevated accumulation in the liver due to uptake by phagocytic cells and/or liver sinusoidal endothelial cells [55,56]. It should be noted, however, that T/N ratio of HA-dOG-PTX-PM even in the liver was 7-fold higher than that of Taxol (Fig. 4E). It is evident, therefore, that HA-dOG-PTX-PM has superior targetability to CD44 positive tumors.

3.5. *In vivo therapeutic efficacy of HA-dOG-PTX-PM*

Finally, we have evaluated the therapeutic performance of HA-

dOG-PTX-PM using MCF-7 human breast tumor-bearing nude mice. The mice were treated with HA-dOG-PTX-PM or Taxol (5.0 mg PTX equiv./kg) when tumors grew up to about 50 mm^3 in volume. The treatment was repeated every three days. Mice received PBS were used as a control. The results showed that HA-dOG-PTX-PM effectively inhibited tumor progression (Fig. 5A). In contrast, continued tumor growth was observed for mice treated with Taxol. The relative tumor volume at day 29 was 0.85, 2.68, and 4.80 for mice treated with HA-dOG-PTX-PM, Taxol and PBS, respectively (Fig. 5A). The photographs of tumor blocks isolated at day 29 confirmed obvious shrinkage of tumor by HA-dOG-PTX-PM (Fig. 5B). Fig. 5C reveals that HA-dOG-PTX-PM did not cause adverse effect. Kaplan–Meier survival curves showed that mice treated with HA-dOG-PTX-PM all survived within an experimental period of 55 d while those with Taxol or PBS all died within 45 d (Fig. 5D).

The maximum tolerated dose (MTD) was assessed in tumor-free mice. The mice were injected with different doses of HA-dOG-PTX-PM or Taxol. The results showed that HA-dOG-PTX-PM was well tolerated at dosages ranging from 20, 50, to 100 mg PTX equiv./kg without abnormal signs and body weight loss within a period of 14 d. However, several abnormal signs such as convulsion and retarded motion were noticed in all the mice immediately following injection of Taxol at a dosage of 20 mg PTX equiv./kg. The high MTD of HA-dOG-PTX-PM is consistent with its excellent stability and low adverse effects, which provides a much broader therapeutic window for effective treatment [50,57].

The histological analyses of tumor and several healthy organs of mice following treatment were performed using TUNEL or H&E staining (Fig. 5E). TUNEL assays revealed that HA-dOG-PTX-PM induced widespread apoptosis of tumor cells. H&E staining showed that HA-dOG-PTX-PM caused severe necrosis in the tumor tissue with little damage to the liver. In contrast, less tumor cell death but more significant liver damage was observed for mice treated with Taxol. These results confirm that HA-dOG-PTX-PM could actively target to CD44 positive human breast tumor xenografts, kill cancer cells by both apoptosis and necrosis mechanisms, and spare the side effects of drug.

4. Conclusions

We have demonstrated that novel hyaluronic acid-shelled acid-activatable paclitaxel prodrug micelles based on hyaluronic acid-*b*-dendritic oligoglycerol block copolymer efficiently target and treat CD44-positive human breast tumor xenografts *in vivo*, affording a 100% progression-free survival rate over an experimental period of 55 day. These smart paclitaxel prodrug micelles possess several unique features: (i) they contain a high drug content (20.6 *wt.*% PTX) due to the multivalency of dendritic oligoglycerol; (ii) they exhibit a remarkably high accumulation and retention in the CD44 receptor-overexpressing tumor following *i.v.* injection (6.19%ID/g at 12 h) likely owing to their active tumor-targeting effect; (iii) they can be rapidly internalized by CD44-positive tumor cells via a receptor-mediated endocytosis mechanism, and release PTX in a pristine state under the endosomal pH conditions, resulting in superior antitumor effect in CD44-positive human breast tumor xenografts with little side effects; and (iv) they display a remarkably high maximum tolerated dose of over 100 mg PTX equiv./kg, which is more than 5 times higher than Taxol. These hyaluronic acid-shelled acid-activatable paclitaxel prodrug micelles with excellent targetability to CD44-possive tumors, high antitumor efficacy, low side effects and high maximum tolerated dose have appeared as a highly promising platform for CD44-targeted cancer chemotherapy.

Acknowledgments

This work is financially supported by research grants from the National Natural Science Foundation of China (NSFC 51273139, 51373113 and 51473110), the National Science Fund for Distinguished Young Scholars (NSFC 51225302), a Project Funded by the Priority Academic Program Development of Jiangsu Higher Education Institutions (PAPD), Jiangsu Higher Education Excellent Science and Technology Innovation Team Program, and Innovative Graduate Research Program of Jiangsu Province (CXZZ13_0805). Z.Z. thanks the Friedrich Wilhelm Bessel Research Award from the Alexander von Humboldt Foundation.

Appendix A. Supplementary data

Supplementary data related to this article can be found at http://dx.doi.org/10.1016/j.biomaterials.2016.01.049.

References

[1] M. Srinivasarao, C.V. Galliford, P.S. Low, Principles in the design of ligand-targeted cancer therapeutics and imaging agents, Nat. Rev. Drug Discov. 14 (2015) 203–219.
[2] V.P. Torchilin, Multifunctional, stimuli-sensitive nanoparticulate systems for drug delivery, Nat. Rev. Drug Discov. 13 (2014) 813–827.
[3] C. Deng, Y. Jiang, R. Cheng, F. Meng, Z. Zhong, Biodegradable polymeric micelles for targeted and controlled anticancer drug delivery: promises, progress and prospects, Nano Today 7 (2012) 467–480.
[4] M. Elsabahy, K.L. Wooley, Design of polymeric nanoparticles for biomedical delivery applications, Chem. Soc. Rev. 41 (2012) 2545–2561.
[5] S. Mura, J. Nicolas, P. Couvreur, Stimuli-responsive nanocarriers for drug delivery, Nat. Mater. 12 (2013) 991–1003.
[6] R. Cheng, F. Meng, C. Deng, Z. Zhong, Bioresponsive polymeric nanotherapeutics for targeted cancer chemotherapy, Nano Today 10 (2015) 656–670.
[7] H. Cabral, K. Kataoka, Progress of drug-loaded polymeric micelles into clinical studies, J. Control Release 190 (2014) 465–476.
[8] Y. Min, J.M. Caster, M.J. Eblan, A.Z. Wang, Clinical translation of nanomedicine, Chem. Rev. 115 (2015) 11147–11190.
[9] A. Wicki, D. Witzigmann, V. Balasubramanian, J. Huwyler, Nanomedicine in cancer therapy: challenges, opportunities, and clinical applications, J. Control Release 200 (2015) 138–157.
[10] V. Delplace, P. Couvreur, J. Nicolas, Recent trends in the design of anticancer polymer prodrug nanocarriers, Polym. Chem. 5 (2014) 1529–1544.
[11] X. Ma, X. Huang, Z. Moore, G. Huang, J.A. Kilgore, Y. Wang, et al., Esterase-activatable β-lapachone prodrug micelles for NQO1-targeted lung cancer therapy, J. Control Release 200 (2015) 201–211.
[12] X. Zhang, K. Achazi, D. Steinhilber, F. Kratz, J. Dernedde, R. Haag, A facile approach for dual-responsive prodrug nanogels based on dendritic polyglycerols with minimal leaching, J. Control Release 174 (2014) 209–216.
[13] J. Liu, W. Liu, I. Weitzhandler, J. Bhattacharyya, X. Li, J. Wang, et al., Ring-opening polymerization of prodrugs: a versatile approach to prepare well-defined drug-loaded nanoparticles, Angew. Chem. Inter Ed. 54 (2015) 1002–1006.
[14] H. Han, H. Wang, Y. Chen, Z. Li, Y. Wang, Q. Jin, et al., Theranostic reduction-sensitive gemcitabine prodrug micelles for near-infrared imaging and pancreatic cancer therapy, Nanoscale 8 (2016) 283–291.
[15] M. Talelli, M. Iman, A.K. Varkouhi, C.J. Rijcken, R.M. Schiffelers, T. Etrych, et al., Core-crosslinked polymeric micelles with controlled release of covalently entrapped doxorubicin, Biomaterials 31 (2010) 7797–7804.
[16] Y. Miura, T. Takenaka, K. Toh, S. Wu, H. Nishihara, M.R. Kano, et al., Cyclic RGD-linked polymeric micelles for targeted delivery of platinum anticancer drugs to glioblastoma through the blood–brain tumor barrier, ACS Nano 7 (2013) 8583–8592.
[17] Z. Zhang, L. Mei, S.-S. Feng, Paclitaxel drug delivery systems, Expert Opin. Drug Deliv. 10 (2013) 325–340.
[18] T. Lammers, F. Kiessling, W.E. Hennink, G. Storm, Drug targeting to tumors: principles, pitfalls and (pre-) clinical progress, J. Control Release 161 (2012) 175–187.
[19] J. Rautio, H. Kumpulainen, T. Heimbach, R. Oliyai, D. Oh, T. Järvinen, et al., Prodrugs: design and clinical applications, Nat. Rev. Drug Discov. 7 (2008) 255–270.
[20] B.S. Tucker, B.S. Sumerlin, Poly (N-(2-hydroxypropyl) methacrylamide)-based nanotherapeutics, Polym. Chem. 5 (2014) 1566–1572.
[21] C. Li, D.-F. Yu, R.A. Newman, F. Cabral, L.C. Stephens, N. Hunter, et al., Complete regression of well-established tumors using a novel water-soluble poly (L-glutamic acid)-paclitaxel conjugate, Cancer Res. 58 (1998) 2404–2409.
[22] F. Leonelli, A. La Bella, L.M. Migneco, R.M. Bettolo, Design, synthesis and applications of hyaluronic acid-paclitaxel bioconjugates, Molecules 13 (2008)

360–378.
[23] Y. Gu, Y. Zhong, F. Meng, R. Cheng, C. Deng, Z. Zhong, Acetal-linked paclitaxel prodrug micellar nanoparticles as a versatile and potent platform for cancer therapy, Biomacromolecules 14 (2013) 2772–2780.
[24] B. Louage, Q. Zhang, N. Vanparijs, L. Voorhaar, S. Vande Casteele, Y. Shi, et al., Degradable ketal-based block copolymer nanoparticles for anticancer drug delivery: a systematic evaluation, Biomacromolecules 16 (2014) 336–350.
[25] H. Wei, R.-X. Zhuo, X.-Z. Zhang, Design and development of polymeric micelles with cleavable links for intracellular drug delivery, Prog. Polym. Sci. 38 (2013) 503–535.
[26] R. Liu, Y. Zhang, X. Zhao, A. Agarwal, L.J. Mueller, P. Feng, pH-responsive nanogated ensemble based on gold-capped mesoporous silica through an acid-labile acetal linker, J. Am. Chem. Soc. 132 (2010) 1500–1501.
[27] W. Chen, P. Zhong, F. Meng, R. Cheng, C. Deng, J. Feijen, et al., Redox and pH-responsive degradable micelles for dually activated intracellular anticancer drug release, J. Control Release 169 (2013) 171–179.
[28] S. Barua, S. Mitragotri, Challenges associated with penetration of nanoparticles across cell and tissue barriers: a review of current status and future prospects, Nano Today 9 (2014) 223–243.
[29] Y. Zhong, F. Meng, C. Deng, Z. Zhong, Ligand-directed active tumor-targeting polymeric nanoparticles for cancer chemotherapy, Biomacromolecules 15 (2014) 1955–1969.
[30] L. Zhu, T. Wang, F. Perche, A. Taigind, V.P. Torchilin, Enhanced anticancer activity of nanopreparation containing an MMP2-sensitive PEG-drug conjugate and cell-penetrating moiety, Proc. Natl. Acad. Sci. U. S. A. 110 (2013) 17047–17052.
[31] J. Fan, G. Fang, F. Zeng, X. Wang, S. Wu, Water-dispersible fullerene aggregates as a targeted anticancer prodrug with both chemo-and photodynamic therapeutic actions, Small 9 (2013) 613–621.
[32] N. Graf, D.R. Bielenberg, N. Kolishetti, C. Muus, J. Banyard, O.C. Farokhzad, et al., $\alpha_V\beta_3$ integrin-targeted PLGA-PEG nanoparticles for enhanced anti-tumor efficacy of a Pt (IV) prodrug, ACS Nano 6 (2012) 4530–4539.
[33] S. Dhar, F.X. Gu, R. Langer, O.C. Farokhzad, S.J. Lippard, Targeted delivery of cisplatin to prostate cancer cells by aptamer functionalized Pt (IV) prodrug-PLGA–PEG nanoparticles, Proc. Natl. Acad. Sci. U. S. A. 105 (2008) 17356–17361.
[34] A. Satsangi, S.S. Roy, R.K. Satsangi, R.K. Vadlamudi, J.L. Ong, Design of a paclitaxel prodrug conjugate for active targeting of an enzyme upregulated in breast cancer cells, Mol. Pharm. 11 (2014) 1906–1918.
[35] H.S. Han, T. Thambi, K.Y. Choi, S. Son, H. Ko, M.C. Lee, et al., Bioreducible shell-cross-linked hyaluronic acid nanoparticles for tumor-targeted drug delivery, Biomacromolecules 16 (2015) 447–456.
[36] C. Yang, X. Wang, X. Yao, Y. Zhang, W. Wu, X. Jiang, Hyaluronic acid nanogels with enzyme-sensitive cross-linking group for drug delivery, J. Control Release 205 (2015) 206–217.
[37] H.S. Min, S. Son, T.W. Lee, H. Koo, H.Y. Yoon, J.H. Na, et al., Liver-specific and echogenic hyaluronic acid nanoparticles facilitating liver cancer discrimination, Adv. Func. Mater. 23 (2013) 5518–5529.
[38] K.-M. Choi, M. Jang, J.H. Kim, H.J. Ahn, Tumor-specific delivery of siRNA using supramolecular assembly of hyaluronic acid nanoparticles and 2b RNA-binding protein/siRNA complexes, Biomaterials 35 (2014) 7121–7132.
[39] X. Deng, M. Cao, J. Zhang, K. Hu, Z. Yin, Z. Zhou, et al., Hyaluronic acid-chitosan nanoparticles for co-delivery of MiR-34a and doxorubicin in therapy against triple negative breast cancer, Biomaterials 35 (2014) 4333–4344.
[40] Y. He, Y. Nie, G. Cheng, L. Xie, Y. Shen, Z. Gu, Viral mimicking ternary polyplexes: a reduction-controlled hierarchical unpacking vector for gene delivery, Adv. Mater. 26 (2014) 1534–1540.
[41] Y. Zhong, J. Zhang, R. Cheng, C. Deng, F. Meng, F. Xie, et al., Reversibly crosslinked hyaluronic acid nanoparticles for active targeting and intelligent delivery of doxorubicin to drug resistant CD44+ human breast tumor xenografts, J. Control Release 205 (2015) 144–154.
[42] G. Jiang, K. Park, J. Kim, K.S. Kim, S.K. Hahn, Target specific intracellular delivery of siRNA/PEI–HA complex by receptor mediated endocytosis, Mol. Pharm. 6 (2009) 727–737.
[43] J. Zhu, X. Shi, Dendrimer-based nanodevices for targeted drug delivery applications, J. Mater. Chem. B 1 (2013) 4199–4211.
[44] Y. Wang, R. Guo, X. Cao, M. Shen, X. Shi, Encapsulation of 2-methoxyestradiol within multifunctional poly(amidoamine) dendrimers for targeted cancer therapy, Biomaterials 32 (2011) 3322–3329.
[45] F. Fu, Y. Wu, J. Zhu, S. Wen, M. Shen, X. Shi, Multifunctional lactobionic acid-modified dendrimers for targeted drug delivery to liver cancer cells: investigating the role played by PEG spacer, ACS Appl. Mater. Interfaces 6 (2014) 16416–16425.
[46] J. Khandare, M. Calderón, N.M. Dagia, R. Haag, Multifunctional dendritic polymers in nanomedicine: opportunities and challenges, Chem. Soc. Rev. 41 (2012) 2824–2848.
[47] H. Zhang, M.W. Grinstaff, Recent advances in glycerol polymers: chemistry and biomedical applications, Macromol. Rapid Commun. 35 (2014) 1906–1924.
[48] M. Calderón, P. Welker, K. Licha, I. Fichtner, R. Graeser, R. Haag, et al., Development of efficient acid cleavable multifunctional prodrugs derived from dendritic polyglycerol with a poly(ethylene glycol) shell, J. Control Release 151 (2011) 295–301.
[49] M. Wyszogrodzka, R. Haag, A convergent approach to biocompatible polyglycerol "click" dendrons for the synthesis of modular core–shell architectures and their transport behavior, Chem. Eur. J. 14 (2008) 9202–9214.
[50] J. Lu, Y. Huang, W. Zhao, R.T. Marquez, X. Meng, J. Li, et al., PEG-derivatized embelin as a nanomicellar carrier for delivery of paclitaxel to breast and prostate cancers, Biomaterials 34 (2013) 1591–1600.
[51] J. Xiong, F. Meng, C. Wang, R. Cheng, Z. Liu, Z. Zhong, Folate-conjugated crosslinked biodegradable micelles for receptor-mediated delivery of paclitaxel, J. Mater. Chem. 21 (2011) 5786–5794.
[52] W. Wang, H. Sun, F. Meng, S. Ma, H. Liu, Z. Zhong, Precise control of intracellular drug release and anti-tumor activity of biodegradable micellar drugs via reduction-sensitive shell-shedding, Soft Matter 8 (2012) 3949–3956.
[53] Y. Matsumura, K. Kataoka, Preclinical and clinical studies of anticancer agent-incorporating polymer micelles, Cancer Sci. 100 (2009) 572–579.
[54] L. Zhou, R. Cheng, H. Tao, S. Ma, W. Guo, F. Meng, et al., Endosomal pH-activatable poly (ethylene oxide)-graft-doxorubicin prodrugs: synthesis, drug release, and biodistribution in tumor-bearing mice, Biomacromolecules 12 (2011) 1460–1467.
[55] H.S. Han, J. Lee, H.R. Kim, S.Y. Chae, M. Kim, G. Saravanakumar, et al., Robust PEGylated hyaluronic acid nanoparticles as the carrier of doxorubicin: mineralization and its effect on tumor targetability in vivo, J. Control Release 168 (2013) 105–114.
[56] K.Y. Choi, K.H. Min, H.Y. Yoon, K. Kim, J.H. Park, I.C. Kwon, et al., PEGylation of hyaluronic acid nanoparticles improves tumor targetability in vivo, Biomaterials 32 (2011) 1880–1889.
[57] K. Xiao, J. Luo, W.L. Fowler, Y. Li, J.S. Lee, L. Xing, et al., A self-assembling nanoparticle for paclitaxel delivery in ovarian cancer, Biomaterials 30 (2009) 6006–6016.